Fusion Engineering and Design 196 (2023) 114004

Contents lists available at ScienceDirect

Fusion Engineering and Design

journal homepage: www.elsevier.com/locate/fusengdes

Corrosion of reduced activation ferritic-martensitic steel – Tungsten brazed joints in liquid lithium

N. Popov [*,a], D. Bachurina [a], R. Bogdanov [a], I. Kozlov [a,b], P. Dzhumaev [a], O. Sevryukov [a], A. Suchkov [a], O. Krutikova [a]

[a] Department of Materials Science, National Research Nuclear University MEPhI, Moscow 115409, Russia
[b] National Research Center "Kurchatov Institute", Moscow 123182, Russia

ARTICLE INFO

Keywords:
Reduced activation ferritic-martensitic steel
Liquid metal corrosion
Lithium
Vacuum brazing
Tungsten

ABSTRACT

Brazed joints between tungsten and steel are the essential part of the divertor armor block. Meanwhile, liquid Li is considered as a prospective coolant and plasma facing material. Therefore, it is important to estimate the corrosion rate of the brazed seam. Corrosion mechanism in liquid Li at 600 °C after 100 h exposure investigated on two types of brazed joints: with Cu and with TiZrBe filler metals. Severe corrosion damage and corrosion failure occur on the brazed seam with Cu filler. Corrosion primarily affects Cu phases in brazed seam. The brazed joint with TiZrBe filler metal shows high corrosion resistance. Results of chemical analysis indicates that corrosion products deposited on specimen surface contain high Fe and Cr content. The corrosion mechanism is similar to corrosion of steel. Corrosion in liquid Li causes preliminary dissolution of Cr-containing phases.

1. Introduction

The future fusion systems are strongly affected by high heat load. Plasma facing component (PFC) in next generation applications such as DEMO and ITER are required to withstand long plasma pulses, overloads and plasma disruptions. Heat flux on a PFC could reach 20 MW/m^2 [1,2]. Due to water thermophysical properties, conventional cooling systems are unable to absorb and remove heat from heavy loaded surfaces [3]. In terms of heat absorption, liquid metals show better performance [4–6].

Beside that liquid metal walls have been proposed to address the issue of PFC compatibility with plasma [7,8]. Nowadays various tokamak concepts and designs use liquid metal as a coolant and breeder material [6,9–14]. One of the most prospective liquid metal is lithium due to its ability to act as a breeder, good physical and thermal properties and shielding [10,15,16]. In addition, lithium is feasible for capillary porous system (CPS), the concept which is one of the major approaches to a problem of interaction between plasma and PFC [10,14,17]. However, there are some limitations in terms of compatibility of liquid Li with structural materials.

Tokamak divertor was designed to remove heavy particles from plasma, therefore it is the most heavily loaded system in tokamak [18]. Divertor constructed of a tungsten armor block joined with base structural material – reduced activation ferrite/martensite (RAFM) steel. To join tungsten to steel high temperature vacuum brazing is used [19].

The most common filler metal for joining W and steel is Cu-based alloys [20,21]. Alternatively brazing can be performed via Ti-based brazing alloys with high reactivity [22,23]. However Cu have an extremely high dissolution rate in liquid lithium [24], thus Cu-containing brazed joints should have low corrosion resistance.

Interaction between most of all fusion-relevant material and liquid Li already was investigated in series of articles [25–28]. However, corrosion resistance in liquid Li of brazed joints, which are supposed to operate in contact with coolant in liquid wall tokamak design, have not been studied yet. Local corrosion of brazed joint could significantly affect the heat transfer which lead to malfunction of entire system. Therefore, corrosion test of brazed joints is a topical problem. In this work corrosion was studied at maximum working temperature of liquid Li – 600 °C [15,29].

2. Material and methods

Tungsten (99.96 wt.%) and Rusfer EK-181 (Fe-12Cr-2W-V-Ta-B wt.%) steel were joined via high temperature vacuum brazing with Ti-48Zr-4Be (wt.%) alloy. To decrease difference in CTE, pure Ta interlayer between W and steel was used. Brazing alloy in form of amorphous foil

* Corresponding author.
E-mail address: NSPopov@mephi.ru (N. Popov).

https://doi.org/10.1016/j.fusengdes.2023.114004
Received 25 May 2023; Received in revised form 31 August 2023; Accepted 11 September 2023
Available online 20 September 2023

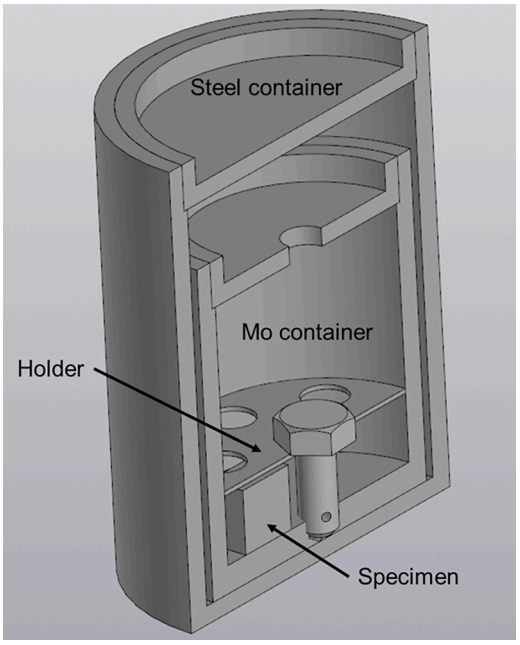

Fig. 1. 3D visualization of the container before corrosion test in liquid Li.

placed between W and Ta and also between Ta and steel. Brazing conducted using mode 1100 °C – 60 min with additional exposure at 720 °C – 180 min to decrease thermal stress. Alternative combination with pure Cu (99,9 wt.%) with a thickness of 0.1 mm was brazed without Ta interlayer.

To estimate the corrosion resistance of brazed joint specimens were placed in the special container. Container design is shown in Fig. 1, it consists of two hollow cylinders. Molybdenum container with specimens, holder and lithium were sealed inside steel container. Due to highly reactive nature of lithium, lithium was injected as a liquid droplet in argon atmosphere. Further steel container cover was welded inside argon box.

Corrosion test were performed in pure liquid Li (99.954 wt.% of Li with N content less than 0.01 wt.%, O_2 content – unknown) at 600 °C during 100 h thermal exposure. The ratio between liquid Li volume and specimens area was more than 90 mm^3/1 mm^2. Additional purification by Zr chips sealed inside container with liquid Li allow to decrease oxygen and nitrogen content. The container with specimen to be tested placed inside muffle furnace. In initial conditions container was in turn over position, so that lithium have not contact with specimen, but in contact with Zr chips. On achieving exposure temperature container was turned over, thus Li melt start to contact with specimen.

To clean specimens surface after immersion in liquid Li, they were immersed in mixture of distilled water and alcohol. Dissolution in alcohol solution increases the operation safety. The procedure finishes with hydrogen desorption via annealing in vacuum 5×10^{-5} Torr at 600 °C during 2 h. Cleaning followed by cutting via IsoMet Low Speed Precision Cutter (with a speed 180 rpm) and common polishing technique for microstructure investigation.

Cutting and microstructure investigation scheme is shown in Fig. 2. Microstructure was investigated via Scanning Electron Microscopy (SEM) on Carl Zeiss EVO 50 XVP and JEOL JSM–6610LV. Qualitative elemental analysis performed using Energy Dispersion Spectrometry (EDS) on Oxford Instruments INCA x-act. Corrosion product structure studied via Transmission Electron Microscope (TEM) Carl Zeiss Libra 120 with an Oxford Instruments X-Max 80T EDX detector.

3. Results

3.1. Corrosion of W/Cu/EK181 joint

All specimens were brazed according temperature/time mode 1100/60+720/180, which was tested in our previous work [30]. As it was mentioned earlier, brazing with Cu-based filler metals allows to obtain direct joints (without interlayer) between W and steel. These joints expected to be vulnerable to Li environment. The corrosion test in liquid Li at 600 °C during 100 h was conducted to measure corrosion rate and to describe the corrosion mechanism.

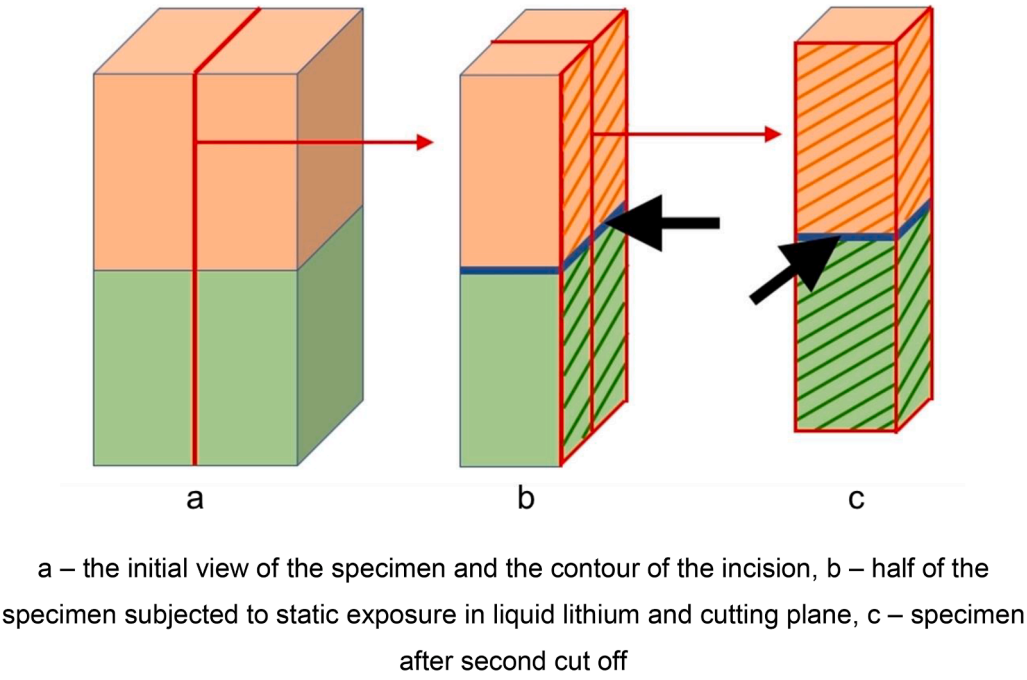

Fig. 2. . Schematic representation of brazed joint specimen for corrosion tests in lithium
a – the initial view of the specimen and the contour of the incision, b – half of the specimen subjected to static exposure in liquid lithium and cutting plane, c – specimen after second cut off.

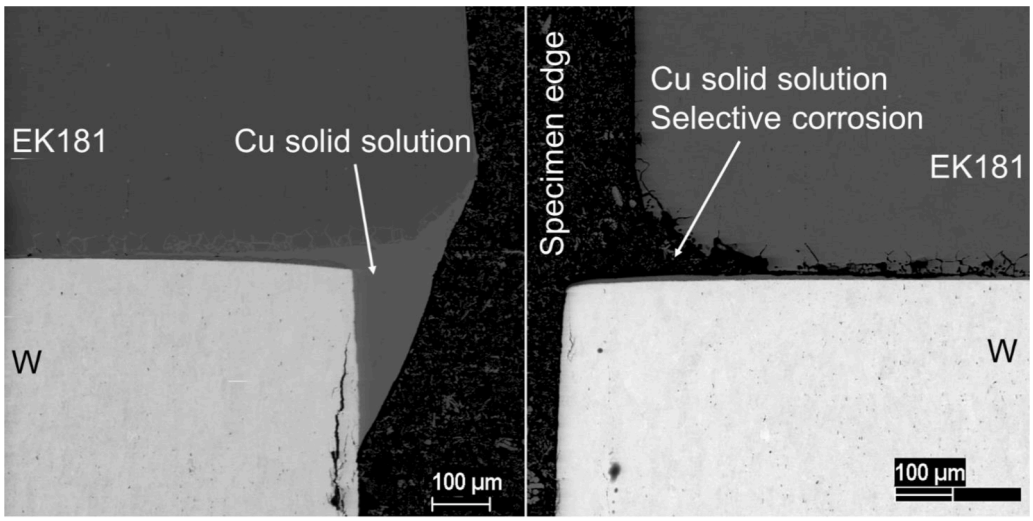

Fig. 3. W/Cu/EK181 joint before (a) and after (b) corrosion in Li at 600 °C during 100 h, edge of brazing seam, which was in contact with liquid Li.

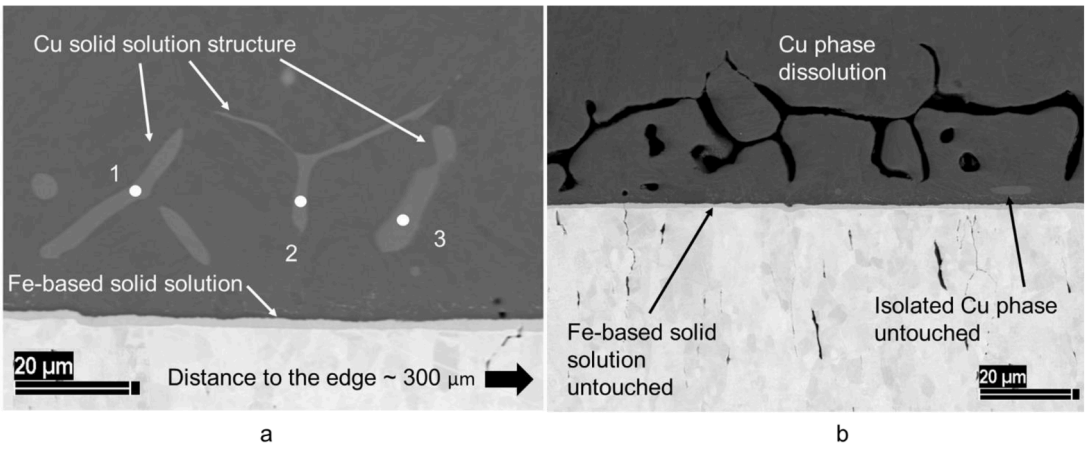

Fig. 4. W/Cu/EK181 joint before (a) and after (b) corrosion in Li at 600 °C during 100 h, seam center area.

Fig. 3 shows the comparison between two parts of one specimen. Before immersion in liquid Li specimen was cut so the first half become the reference specimen and the second one was used in the corrosion test. Initial W/Cu/EK181 brazed seam edge is shown in Fig. 3a, this specimen was not exposed to liquid Li. Copper layer is clearly visible at the brazed seam center. After 100 h of exposure this layer was selectively leached which resulted in almost complete failure of brazed seam. One of the specimens exposed to liquid Li fall apart during low speed cutting.

To describe the corrosion failure mechanism more detailed analysis of initial brazed seam was carried out. According to EDS analysis shown in Fig. 4, selective corrosion affects phases marked on the image with chemical composition of 88Cu-9.7Fe-1.5Cr-0.8Mn at.%. These phases identify as Cu-based solid solution, which forms during brazing.

As it was reported earlier in [20] Fe-based solid solution crystallize on the W side of the seam. Apparently, this zone has higher corrosion resistance to liquid Li than Cu-based phases.

After exposure to liquid Li for 100 h, the average weight loss of the three specimens was 0.01817 g. Correct evaluation of corrosion rate is quite difficult due to unknown area of the copper subject to corrosion damage. The only way to estimate the area of corroded Cu, is to assume it is close to the end face area of the initial Cu brazing alloy. Hence the area of brazed seam was 2.8 mm^2 and the weight loss rate equals 6489 $g*m^{-2}$. This corresponds with a weight loss rate of 6991.5 $g*m^{-2}$ for pure copper reported in [24]. Still due to methodological limitations this value cannot be considered as correct.

3.2. *Corrosion of W/TiZr4Be/Ta joint*

Corrosion tests of W/TiZr4Be/EK-181 with Ta interlayer brazed joint (mode 1100/60+720/180) in liquid Li were carried out at a temperature of 600 °C. Specimens were immersed in liquid Li for 100 h. Results and discussion will be divided into 2 main parts, first one about brazed joint between W and Ta, second one about Ta/EK-181 brazed joint Comprehensive phase analysis of brazed joint given in [30].

It should be noted that filler metal melt from the gap between W and Ta mix with the melt from the gap between Ta and EK-181. This occur due to TiZr4Be alloy high reactivity. After filling the space between brazed materials, redundant melt starts to wet the side face of the specimen. As a result, melt from W/Ta joint contact and mix with melt from Ta/EK-181 joint.

Fig. 5 shows the microstructure of the joint surface after contact with liquid Li. Corrosive products form on the surface. Few areas with signs of corrosion damage and with corrosion products can be observed on brazed seam.

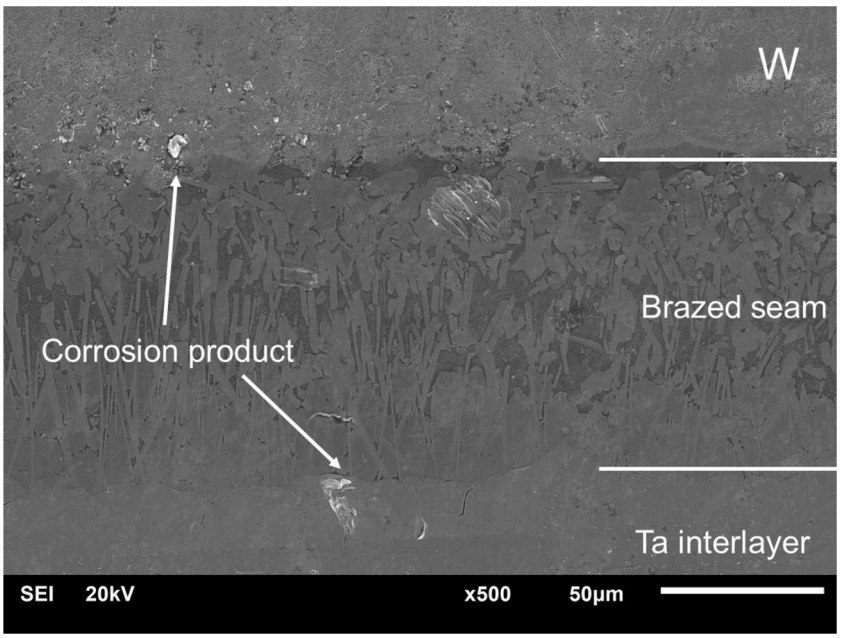

Fig. 5. SEM image of front side of the brazed seam W/TiZr4Be/Ta after exposure in Li at 600 °C during 100 h.

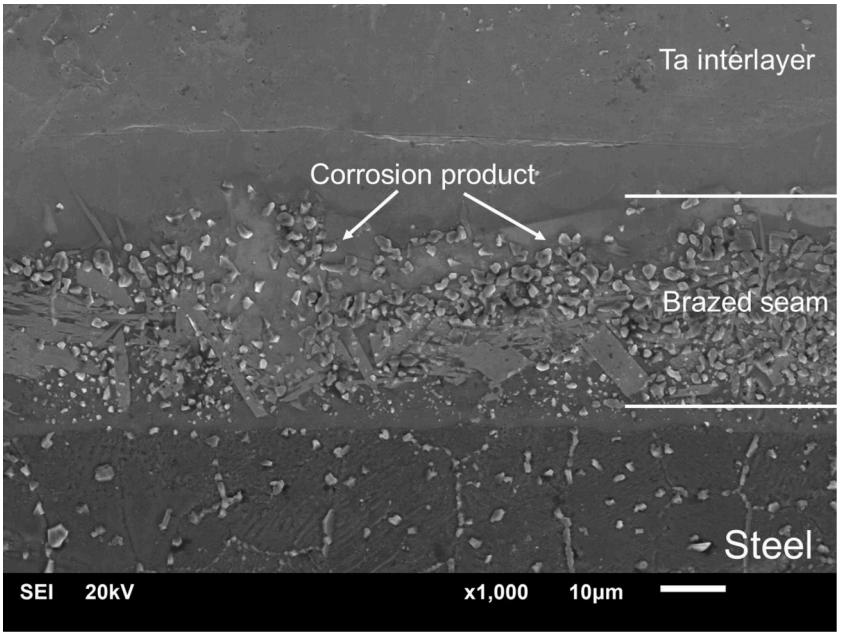

Fig. 6. SEM image of front side of the specimens after exposure in Li at 600 °C during 100 h.

3.3. Corrosion of Ta/TiZr4Be/EK-181 joint

Brazed joint Ta/TiZr4Be/EK-181, shown in Fig. 6, demonstrates high resistance to corrosion attack, however, some corrosive products in form of crystals were observed on the surface of steel and on the brazed seam. Identification of the chemical composition of these corrosion product via EDS mapping shown in Fig. 7. It shows that Cr–based crystals formed on the steel, and Fe-based crystals formed on the brazed joint surface. Beside that, Cr-based segregations formed on the surface near steel grain boundaries.

3.4. Corrosion depth

The image of cross-section of specimen after corrosion shown in Fig. 8. Investigated specimen consists of polished «face» surface and edge zone (fillet area). Both of them were in contact with Li environment. Microstructure of the fillet area differs from the rest part of the brazed seam. In practice, particularly this area will contact with liquid Li in operation conditions of real device. Fig. 8a shows the «face» area after contact with Li, Fig. 8b – an edge (fillet) area after corrosion in Li. No visible signs of corrosion damage detected in Fig. 8a. All cracks and pores in Fig. 8b formed after brazing. No signs of crack propagation observed.

3.5. TEM analysis of corrosion products on brazed seam surface

To investigate the structure and chemical composition of corrosion products on specimen surface TEM with additional EDS analysis was

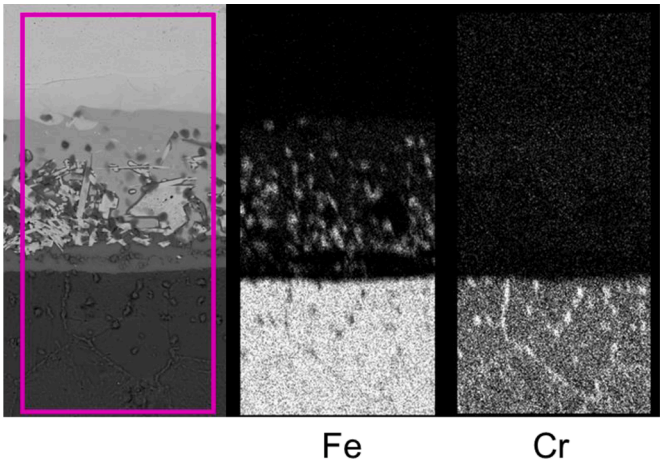

Fig. 7. Chemical analysis map of Ta/TiZr4Be/EK-181 after corrosion test.

used. High magnification image of brazed seam surface shown in Fig. 9. Results of EDS are given in Table 1. According to EDS analysis shown in Fig. 9, segregation (point 2) formed on typical Ti-based solid solution (point 1). It can be clearly observed, that the surface of the segregation has a light shade, which means high content of heavy elements (Ta, Fe).

3.6. TEM analysis of corrosion products on steel surface

Few areas with signs of corrosion damage detected on a steel surface. Image with high magnification of damaged steel surface shown in Fig. 10. Dark phase (point 3) locates right on a steel surface, without any intermediate layer such as observed on brazed seam. EDS identifies it as a chromium carbide.

Further investigations consider oxides on steel surface. Two corrosion affected zones shown in Fig. 11. Steel covered with thin (~20 nm) oxide layer (point 4 on Fig. 11a) with low Cr content. Steel under the oxide (point 5 and point 8 in Fig. 11b with similar composition) depleted by Cr content. The initial Cr content in steel is 11.9 at.% [31], after corrosion it decreased to 8.5 at.%.

In Fig. 11b chromium carbide forms on an oxide layer, which in turn locates on a steel surface. Carbide (point 6) enriched with Cr, that was previously dissolved in liquid Li. Oxide (point 7) under carbide enriched with Cr (18.9 at.%), in opposition to previous case without carbide deposition.

4. Discussion

4.1. Corrosion of W/Cu/EK181 joint

Brazed joint W/Cu/EK181 consists of fillet area and seam area. During brazing redundant filler metal melt squeezes out from the gap forming the fillet. After cooling this liquid solidifies as Cu-based solid solution. As it was shown in Fig. 3b, fillet was completely dissolved by Li.

Copper liquid during brazing react actively with steel EK-181, especially with grain boundaries. Thus Cu-based solid solution mostly solidifies around steel grains, forming tree-like structure. After dissolution of the fillet, Li start to dissolve the seam. Still there is a small number of Cu-based phases that remain untouched by corrosion. They are isolated from tree-like structure. Generally speaking, mechanism described above can be characterized as selective corrosion of Cu-based phases.

4.2. Corrosion of W/Ta/EK-181 joint with TiZrBe filler metal

The joint obtained via brazing with TiZrBe alloy primarily consist of Ti-based solid solution and various intermetallics. Result of EBSD analysis from our previous work [30] shown in Fig. 12. High corrosion resistance of the brazed joint attributes to phase and chemical composition of the seam. Chemical elements as Ti, Ta, Be and Zr by themselves show high resistance to corrosion in liquid Li at this temperature range [26,32,33].

Due to the presence of interlayer between segregation and brazed seam (Fig. 9), it could be concluded, that corrosion product was deposited from liquid Li on a specimen surface. The chemical composition of segregations indicates that corrosion primarily affects the steel surface without significant dissolution of brazed seam. The segregation

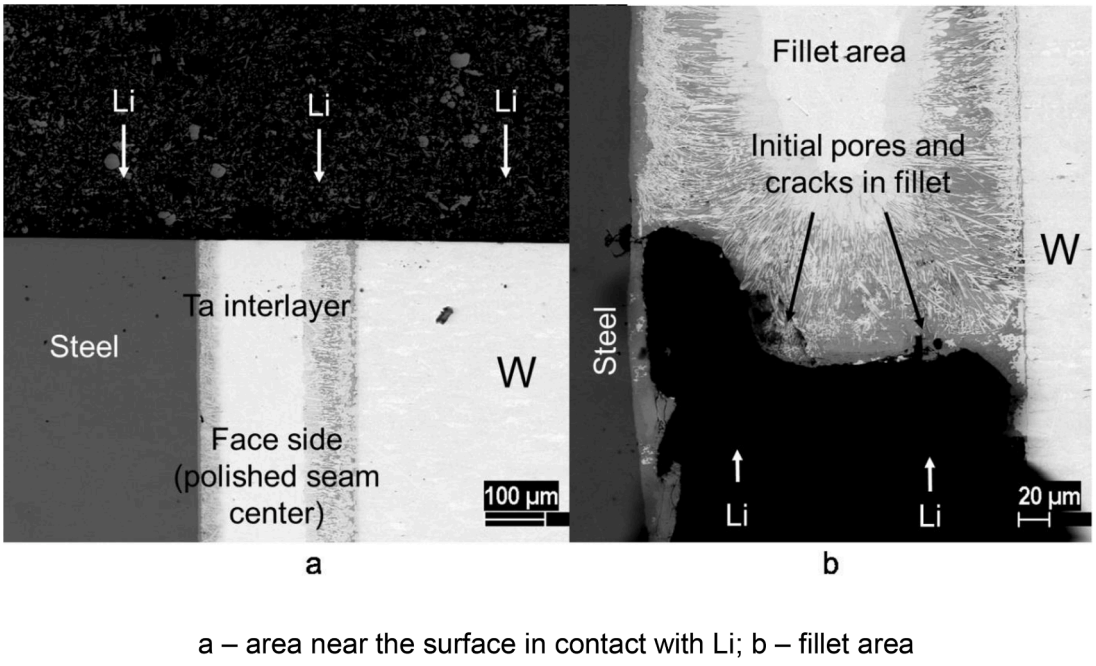

Fig. 8. Cross-section microstructure of specimens after corrosion tests
a – area near the surface in contact with Li; b – fillet area.

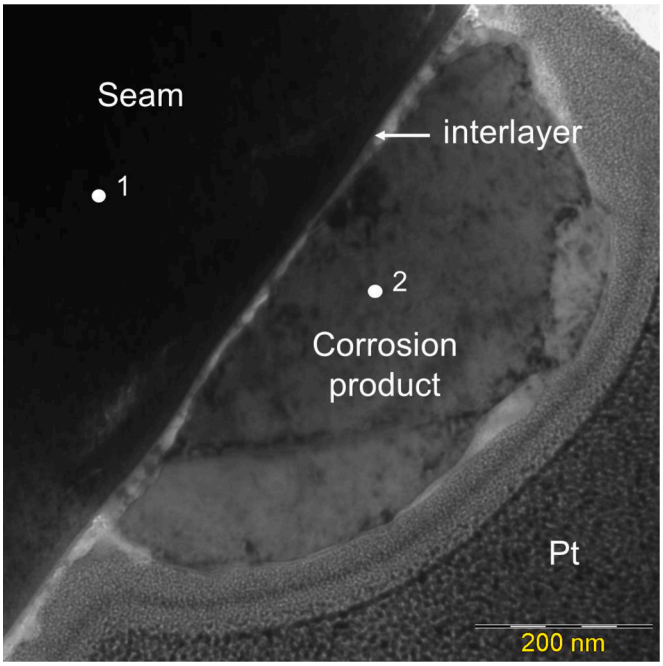

Fig. 9. TEM image of brazed seam surface with segregation on it after corrosion in liquid Li.

contains primarily Fe, C and Cr which are the base elements of the steel. Conversely, the content of chemical elements from the brazed seam, such as Ti, Ta, Zr, is significantly lower.

Exposure in liquid Li causes the formation of ternary chemical compound (Li, Cr, Fe with oxygen, nitrogen and carbon) on the steel surface. Some of these compounds dissolve in liquid Li, in addition to dissolved elements from the specimen's surface. After exposure, cooling follows, during which Fe, Cr and C, previously dissolved in Li, form segregations. A similar mechanism was observed in [34].

The deposition process caused by a decrease in the solubility of elements in liquid Li during the cooling after corrosion tests. After the corrosion tests and cooling, solubility of Cr and C in Li decreases, which causes chromium carbides formation on the steel surface. A significant difference in solubility of chemical elements in liquid Li was reported in [35,36].

The corrosion process in case of brazed joint W/TiZr4Be/Ta/TiZr4Be/EK181 follows a similar mechanism to that of the corrosion of RAFM steels without brazing, investigated in [34,37]. In these studies, corrosion primarily affected grain boundaries, leading to selective corrosion of chromium carbides. This selective corrosion results in a chemical reaction and the formation of Cr carbides on the steel surface. The corrosion process mainly affects steel; the only corrosion effect observed on brazed seam is the deposition of corrosion products on it.

4.3. Further work

This paper aimed to compare corrosion behavior of two different types of brazed seam. Still long-term corrosion experiments are needed to establish the mechanism of corrosion degradation of TiZrBe joint and its evolution. Such investigations as in [38] demonstrate significant difference in corrosion behavior of different RAFM steels. This means that after some period the corrosion mechanism could change from preliminary dissolution of Cr-based phases to corrosion of brazed joint. In addition, depth distribution of Li in corroded material is important information to understand the corrosion process [39]. The penetration of Li in brazed joint could affect the microstructure and joint strength. Common mechanical characterization method for brazed joints is shear test [30].

Our further work will focus on long-term corrosion of TiZrBe joints, chemical elements depth distribution and joint strength after corrosion tests.

5. Conclusions

Corrosion characteristics in liquid Li at 600 °C after 100 h of exposure of two types of brazed joint: with Cu and TiZrBe filler metals were investigated. Local dissolution of Cu-based phases in the joint causes severe damage and malfunction of the joint.

Corrosion tests of brazed joint W/Ta/EK-181 with TiZrBe alloy show high corrosion resistance of brazed joints. Segregations on brazed joint

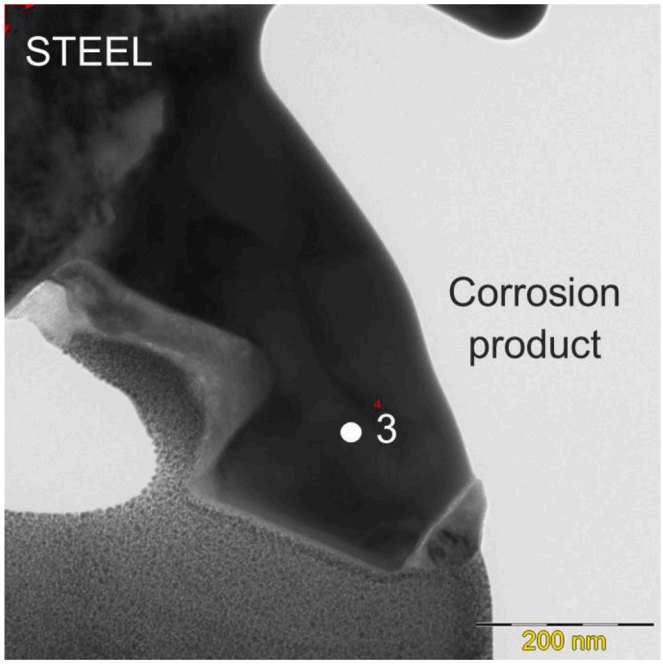

Fig. 10. TEM image of steel surface with carbide after corrosion in liquid Li.

Table 1
Chemical composition of corrosion products.

Point N°	Zone name	Chemical composition, at.%									
		Ti	Zr	Fe	Ta	Cr	O	C	W	Mn	Si
1	Seam	43	17.2	19.5	16.7	3.6	–	–	–	–	–
2	Corrosion product	4.6	0.4	80.9	0.3	1.6	12.2	–	–	–	–
3	Corrosion product	–	–	10.8	–	37.7	9.5	40.3	0.7	1	–
4	Oxide on steel	–	–	51.9	–	6.4	40.3	–	–	0.4	1
5, 8	Steel	–	0.3	64	–	8.5	25.6	–	0.3	0.5	0.8
6	Carbide	–	–	13.1	–	38.1	10.4	37	0.2	1.2	–
7	Oxide on steel	–	–	4.8	–	18.9	73	2.5	0.2	0.6	–

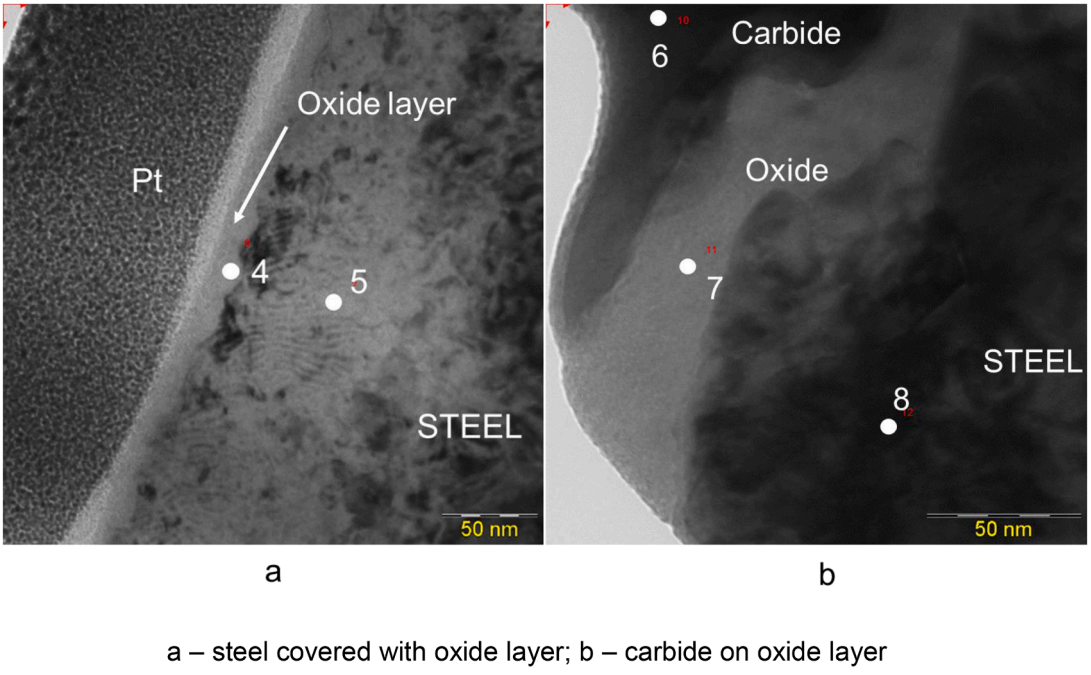

Fig. 11. TEM image of steel surface after corrosion in liquid Li
a – steel covered with oxide layer; b – carbide on oxide layer.

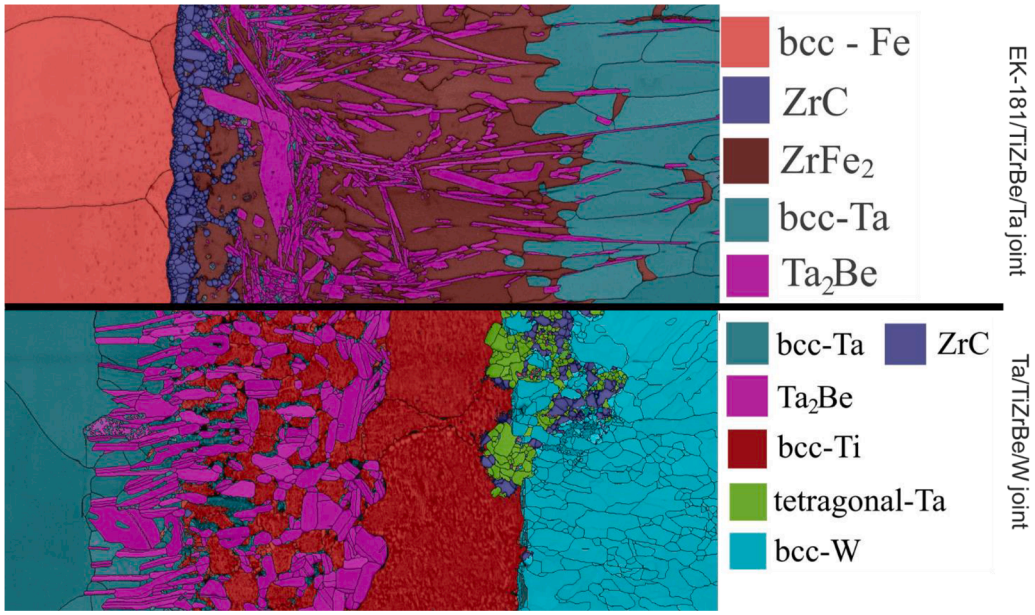

Fig. 12. . EBSD map of W/Ta/EK-181 joint [30].

primarily consist of C with various Cr and Fe content, they form due to the decrease in solubility in liquid Li during cooling. The corrosion mechanism is similar to process on RAFM steel immersed in liquid Li. Corrosion in liquid Li causes preliminary dissolution of Cr-containing phases on steel grain boundaries, after which chemical reaction results in Cr carbides segregation. The corrosion of TiZrBe brazing alloy in liquid Li was less than that of pure Cu filler metal. High corrosion resistance of TiZrBe brazed joint is attributed to high corrosion resistance of the base elements.

Funding

This research did not receive any specific grant from funding agencies in the public, commercial, or not-for-profit sectors.

Declaration of generative Ai and AI-assisted technologies in the writing process

During the preparation of this work the author(s) used OpenAI ChatGPT-4 in order to improve language. After using this tool/service, the author(s) reviewed and edited the content as needed and take(s) full responsibility for the content of the publication.

CRediT authorship contribution statement

N. Popov: Investigation, Methodology, Writing – original draft. **D. Bachurina:** Investigation, Writing – review & editing. **R. Bogdanov:** Conceptualization. **I. Kozlov:** Investigation. **P. Dzhumaev:** Investigation. **O. Sevryukov:** Resources. **A. Suchkov:** Project administration. **O. Krutikova:** Visualization, Writing – original draft.

Declaration of Competing Interest

The authors declare that they have no known competing financial interests or personal relationships that could have appeared to influence the work reported in this paper.

Data availability

Data will be made available on request.

References

[1] G. Federici, W. Biel, M.R. Gilbert, R. Kemp, N. Taylor, R. Wenninger, European DEMO design strategy and consequences for materials, Nucl. Fusion 57 (2017), https://doi.org/10.1088/1741-4326/57/9/092002.

[2] I.V. Mazul, G.L. Saksagansky, First Wall Components, Elsevier Ltd, 2018, https://doi.org/10.1016/b978-0-08-102470-6.00007-x.

[3] Z. Wang, S. Zhang, Z. Chen, J. Jia, C. Chao, A novel liquid lithium jet-cooled finger-type divertor target concept for fusion power plant application, Nucl. Fusion 61 (2021), https://doi.org/10.1088/1741-4326/abe7d1.

[4] K. Natesan, C.B. Reed, R.F. Mattas, Assessment of alkali metal coolants for the ITER blanket, Fusion Eng. Des. 27 (1995) 457–466, https://doi.org/10.1016/0920-3796(95)90159-0.

[5] R.E. Nygren, F.L. Tabarés, Liquid surfaces for fusion plasma facing components—A critical review. Part I: physics and PSI, Nucl. Mater. Energy 9 (2016) 6–21, https://doi.org/10.1016/j.nme.2016.08.008.

[6] P. Rindt, J.L. van den Eijnden, T.W. Morgan, N.J. Lopes Cardozo, Conceptual design of a liquid-metal divertor for the European DEMO, Fusion Eng. Des. 173 (2021), 112812, https://doi.org/10.1016/j.fusengdes.2021.112812.

[7] R. Kaita, L. Berzak, D. Boyle, T. Gray, E. Granstedt, G. Hammett, C.M. Jacobson, A. Jones, T. Kozub, H. Kugel, B. Leblanc, N. Logan, M. Lucia, D. Lundberg, R. Majeski, D. Mansfield, J. Menard, J. Spaleta, T. Strickler, J. Timberlake, J. Yoo, L. Zakharov, R. Maingi, V. Soukhanovskii, K. Tritz, S. Gershman, Experiments with liquid metal walls: status of the lithium tokamak experiment, Fusion Eng. Des. 85 (2010) 874–881, https://doi.org/10.1016/j.fusengdes.2010.04.005.

[8] A. Hançerlioğullari, M. Cini, Different mechanisms for establishing liquid walls in advanced reactor systems, J. Fusion Energy 32 (2013) 155–163, https://doi.org/10.1007/s10894-012-9539-z.

[9] S. Malang, A.R. Raffray, N.B. Morley, An example pathway to a fusion power plant system based on lead-lithium breeder: comparison of the dual-coolant lead-lithium (DCLL) blanket with the helium-cooled lead-lithium (HCLL) concept as initial step, Fusion Eng. Des. 84 (2009) 2145–2157, https://doi.org/10.1016/j.fusengdes.2009.02.049.

[10] V.A. Evtikhin, A.V. Vertkov, I.E. Lyublinski, B.I. Khripunov, V.B. Petrov, S. V. Mirnov, Research of lithium capillary-pore systems for fusion reactor plasma facing components, J. Nucl. Mater. (2002) 1664–1669, https://doi.org/10.1016/S0022-3115(02)01132-7, 307–311.

[11] I.V. Vitkovsky, M.M. Golovanov, V.A. Divavin, I.R. Kirillov, A.V. Lipko, A. A. Malkov, I.A. Kartashev, V.M. Komarov, A.P. Ogorodnikov, O.L. Schipakin, Neutronic, thermal-hydraulic and stress analysis of RF lithium cooled test blanket module for ITER, Fusion Eng. Des. (2000) 703–707, https://doi.org/10.1016/S0920-3796(00)00175-7, 49–50.

[12] R.E. Nygren, T.D. Rognlien, M.E. Rensink, S.S. Smolentsev, M.Z. Youssef, M. E. Sawan, B.J. Merrill, C. Eberle, P.J. Fogarty, B.E. Nelson, D.K. Sze, R. Majeski, A fusion reactor design with a liquid first wall and divertor, Fusion Eng. Des. 72 (2004) 181–221, https://doi.org/10.1016/j.fusengdes.2004.07.007.

[13] F.L. Tabarés, E. Oyarzabal, A.B. Martin-Rojo, D. Tafalla, A. de Castro, F. Medina, M. A. Ochando, B. Zurro, K. McCarthy, Experimental tests of LiSn alloys as potential liquid metal for the divertor target in a fusion reactor, Nucl. Mater. Energy 12 (2017) 1368–1373, https://doi.org/10.1016/j.nme.2016.11.026.

[14] S.V. Mirnov, V.N. Dem'yanenko, E.V. Murav'ev, Liquid-metal tokamak divertors, J. Nucl. Mater. 196–198 (1992) 45–49, https://doi.org/10.1016/S0022-3115(06)80010-3.

[15] I.E. Lyublinski, A.V. Vertkov, V.V. Semenov, Comparative analyses of low melting metals application with capillary-pore systems in tokamak conditions, Probl. At. Sci. Technol. Ser. Thermonucl. Fusion 38 (2015) 7–14, https://doi.org/10.21517/0202-3822-2015-38-1-7-14.

[16] M. Ono, M.G. Bell, Y. Hirooka, R. Kaita, H.W. Kugel, G. Mazzitelli, J.E. Menard, S. V. Mirnov, M. Shimada, C.H. Skinner, F.L. Tabares, Conference report on the 2nd international symposium on lithium applications for fusion devices, Nucl. Fusion 52 (2012), https://doi.org/10.1088/0029-5515/52/3/037001.

[17] I.E. Lyublinski, A.V. Vertkov, M.Y. Zharkov, O.N. Sevryukov, P.S. Dzhumaev, V. A. Shumskiy, A.A. Ivannikov, Selection of materials for tokamak plasma facing elements based on a liquid tin capillary pore system, J. Phys. Conf. Ser. 748 (2016), https://doi.org/10.1088/1742-6596/748/1/012014.

[18] G. Federici, C.H. Skinner, J.N. Brooks, J.P. Coad, C. Grisolia, T. Supra, A.A. Haaszd, V. Philipps, C.S. Pitcherf, J. Roth, D.G. Whyteh, W.R. Wampler, Plasma–material interactions in current tokamaks and their implications for next step fusion reactors, Nucl. Fusion 41 (2001) 1970–1971.

[19] D. Bachurina, X.Y. Tan, F. Klein, A. Suchkov, A. Litnovsky, J. Schmitz, J. Gonzalez-Julian, M. Bram, J.W. Coenen, Y.C. Wu, C. Linsmeier, Self-passivating smart tungsten alloys for DEMO: a progress in joining and upscale for a first wall mockup, Tungsten 3 (2021) 101–115, https://doi.org/10.1007/s42864-021-00079-5.

[20] D. Bachurina, A. Suchkov, A. Filimonov, I. Fedotov, M. Savelyev, O. Sevryukov, B. Kalin, High-temperature brazing of tungsten with steel by Cu-based ribbon brazing alloys for DEMO, Fusion Eng. Des. 146 (2019) 1343–1346, https://doi.org/10.1016/j.fusengdes.2019.02.072.

[21] J. de Prado, M. Sánchez, A. Ureña, Development of brazing process for W–EUROFER joints using Cu-based fillers, Phys. Scr. T167 (2016), 014022, https://doi.org/10.1088/0031-8949/T167/1/014022.

[22] W. Zhu, J. Qiang, Y. Wang, J. Sun, J. Wang, Y. Lian, F. Feng, X. Liu, A Ti-Fe-Sn thin film assembly for joining tungsten and reduced activation ferritic-martensitic steels, Mater. Des. 125 (2017) 55–61, https://doi.org/10.1016/j.matdes.2017.03.060.

[23] B.A. Kalin, A.N. Suchkov, V.T. Fedotov, O.N. Sevryukov, A.A. Ivannikov, A. A. Polyansky, I.V. Mazul, A.N. Makhankov, A.A. Gervash, P.S. Dzhumaev, V. L. Yakushin, V.I. Polsky, Application of rapidly quenched ribbon-type filler metals for brazing of the high-heat-flux elements of ITER, Fusion Sci. Technol. 61 (2012) 147–153, https://doi.org/10.13182/FST12-A13381.

[24] X.C. Meng, C. Xu, G.Z. Zuo, M. Huang, K. Tritz, D. Andruczyk, Z. Sun, W. Xu, Y. Z. Qian, J.J. Huang, X. Gao, B. Yu, J.G. Li, J.S. Hu, H. Deng, Corrosion characteristics of copper in static liquid lithium under high vacuum, J. Nucl. Mater. 513 (2019) 282–292, https://doi.org/10.1016/j.jnucmat.2018.10.037.

[25] W. Xia, L. Yang, K. Zhang, P. He, L. Shu, L. Han, X. Ma, Z. Zhang, Z. Cao, F. Gou, Study of corrosion behaviors of 316L stainless steel welds in liquid lithium with hydrogen impurity, Fusion Sci. Technol. 75 (2019) 104–111, https://doi.org/10.1080/15361055.2018.1533618.

[26] I.B. Kupriyanov, V.N. Kudryavtsev, L.A. Kurbatova, I.E. Lyublinski, Effect of high temperature corrosion in liquid lithium on mechanical properties of beryllium, Fusion Eng. Des. 85 (2010) 1702–1706, https://doi.org/10.1016/j.fusengdes.2010.05.006.

[27] Q. Xu, M. Kondo, T. Nagasaka, T. Muroga, O. Yeliseyeva, Effect of chemical potential of carbon on phase transformation and corrosion of JLF-1 steel in a static lithium, J. Nucl. Mater. 394 (2009) 20–25, https://doi.org/10.1016/j.jnucmat.2009.08.005.

[28] X. Meng, G. Zuo, Z. Sun, W. Xu, M. Huang, C. Xu, Y. Qian, W. Hu, J. Hu, H. Deng, Compatibility of molybdenum, tungsten, and 304 stainless steel in static liquid lithium under high vacuum, Plasma Phys. Rep. 44 (2018) 671–677, https://doi.org/10.1134/S1063780X18070036.

[29] A.V. Vertkov, M.Y. Zharkov, I.E. Lyublinski, A.V. Berlov, I.L. Tazhibayeva, Y. V. Ponkratov, Y.N. Gordienko, New version of lithum divertor of KTM tokamak, Probl. At. Sci. Technol. Ser. Thermonucl. Fusion 42 (2019) 5–13, https://doi.org/10.21517/0202-3822-2019-42-4-5-13.

[30] D. Bachurina, A. Suchkov, J. Gurova, V. Kliucharev, V. Vorkel, M. Savelyev, P. Somov, O. Sevryukov, Brazing tungsten/tantalum/RAFM steel joint for DEMO by fully reduced activation brazing alloy 48Ti-48Zr-4Be, Metals 11 (2021), https://doi.org/10.3390/met11091417 (Basel).

[31] С.Г. Богданов, Б.Н. Гощицкий, В.Д. ПархоМенко, М.В. Леонтьева-СМирнова, В. М. Чернов, Кристаллические и Магнитные структуры Исследование наноструктуры ферритно-Мартенситных 12%-хроМистых сталей МетодоМ Малоуглового рассеяния нейтронов, Физика Твердого Тела 56 (2014) 9–20.

[32] J.R. DiStefano. Corrosion of Refractory Metals By Lithium, Report No. ORNL-3551, Oak Ridge National Laboratory, Oak Ridge, Tennessee, 1964.

[33] R.L. Klueh, Oxygen effects on the corrosion of niobium and tantalum by liquid lithium, Metall. Trans. 5 (1974) 875–879, https://doi.org/10.1007/BF02643141.

[34] M. Kondo, M. Takahashi, T. Tanaka, V. Tsisar, T. Muroga, Compatibility of reduced activation ferritic martensitic steel JLF-1 with liquid metals Li and Pb-17Li, Fusion Eng. Des. 87 (2012) 1777–1787, https://doi.org/10.1016/j.fusengdes.2011.12.013.

[35] I.E. Lyublinski, V.A. Evtikhin, V.Y. Pankratov, V.P. Krasin, Numerical and experimental determination of metallic solubilities in liquid lithium, lithium-containing nonmetallic impurities, lead and lead-lithium eutectic, J. Nucl. Mater. 224 (1995) 288–292, https://doi.org/10.1016/0022-3115(95)00076-3.

[36] M. Kondo, T. Muroga, T. Nagasaka, Q. Xu, V. Tsisar, T. Oshima, Mass transfer of RAFM steel in Li by simple immersion, impeller induced flow and thermal convection, J. Nucl. Mater. 417 (2011) 1200–1204, https://doi.org/10.1016/j.jnucmat.2011.01.096.

[37] Q. Xu, M. Kondo, T. Nagasaka, T. Muroga, M. Nagura, A. Suzuki, Corrosion characteristics of low activation ferritic steel, JLF-1, in liquid lithium in static and

thermal convection conditions, Fusion Eng. Des. 83 (2008) 1477–1483, https://doi.org/10.1016/j.fusengdes.2008.05.034.

[38] V. Tsisar, M. Kondo, T. Muroga, T. Nagasaka, O. Yeliseyeva, Structural and compositional transformations in the near-surface layers of Fe-Cr based steels exposed to lithium - Effect of alloying and corrosion-assisted substructure coarsening, Corros. Sci. 53 (2011) 441–447, https://doi.org/10.1016/j.corsci.2010.09.055.

[39] C. Ke, Y. Li, X. Liu, F. Gou, X. Duan, Y. Zhao, Application of laser induced breakdown spectroscopy for fast depth profiling analysis of type 316 stainless steel parts corroded by liquid lithium, Fusion Eng. Des. 136 (2018) 1647–1652, https://doi.org/10.1016/j.fusengdes.2018.07.004.